Imaging Fluorescence Correlation Spectroscopy: Nonuniform IgE Distributions on Planar Membranes

Zhengping Huang and Nancy L. Thompson
Department of Chemistry, University of North Carolina, Chapel Hill, North Carolina 27599-3290 USA

ABSTRACT Fluorescence correlation spectroscopy is useful for detecting and characterizing molecular clusters that are smaller than or approximately equal to optical resolution in size. Here, we report the development of an approach in which the pixel-to-pixel fluorescence fluctuations from a single fluorescence image are spatially autocorrelated. In these measurements, tetramethylrhodamine-labeled, anti-trinitrophenyl IgE antibodies were specifically bound to substrate-supported planar membranes composed of trinitrophenyl-aminocaproyldipalmitoylphosphatidylethanolamine and dipalmitoylphosphatidylcholine. The antibody-coated membranes were illuminated with the evanescent field from a totally internally reflected laser beam, and the fluorescence arising from the IgE-coated membranes was recorded with a cooled CCD camera. The image was corrected for the elliptical Gaussian shape of the evanescent illumination after background subtraction. The spatial autocorrelation functions of the resulting images generated two useful parameters: the extrapolated initial values, which were related to the average cluster intensity and density; and the correlation distances, which were related to the average cluster size. These parameters varied with the IgE density, and unlabeled polyclonal anti-IgE enhanced the nonuniform IgE distributions. The autocorrelation functions calculated from images of planar membranes containing fluorescently labeled lipids rather than bound, labeled IgE demonstrated that the spatial nonuniformities were prominent only in the presence of IgE. Fluorescent beads were used to demonstrate the principles and the methods.

INTRODUCTION

Molecular events at cell surfaces are central to signal transduction and subsequent cellular response. A physical event that is in many cases thought to modulate signal transduction is the formation of receptor dimers or high-order oligomers (Jans, 1992; Bormann and Engelman, 1992; Grasberger et al., 1986; Ward and Hammer, 1992). Receptor clustering has been implicated or confirmed in a large variety of signal transduction processes, including those mediated by growth factors (Cunningham et al., 1991; Ullrich and Schlessinger, 1990; Fantl et al., 1993) and immune cell receptors (Sette et al., 1994; Young et al., 1983).

A variety of techniques have been employed to characterize the self-association of proteins in or on natural or model membranes. Fluorescence photobleaching methods provide quantitative information about translational (Wright et al., 1988) and rotational (Velez et al., 1990) mobilities; phosphorescence anisotropy methods provide similar information (Matayoshi et al., 1991; Zidovetzki et al., 1991). However, these methods do not provide direct information about aggregation. Electron microscopy has been used to provide structural information about membrane proteins that form ordered two-dimensional arrays (Jap et al., 1992; Kornberg and Darst, 1991), but the sampling conditions are far from physiological and the time resolution is difficult to control. Fluorescence energy transfer methods have yielded qualitative information about receptor clustering in natural cell membranes but have been less successful in yielding quantitative information about cluster size and density (Kubitscheck et al., 1991, 1993; Liang et al., 1993; Szabo et al., 1992; Young et al., 1994). Digital video microscopy can be used to characterize receptor clustering on viable cells if individual clusters are intensely fluorescent and sufficiently sparse to be optically resolved (Ghosh and Webb, 1994; Morrison et al., 1994). If the clusters are less fluorescent or more densely distributed, fluorescence correlation spectroscopy (FCS) may be employed (Thompson, 1991).

In the simplest type of FCS, movement of fluorescent molecules through a small illuminated region generates temporal fluctuations in the fluorescence emitted from the region. The magnitude of the fluorescence fluctuation autocorrelation function is sensitive to the number densities and therefore to the formation of molecular clusters (Palmer and Thompson, 1989a,b). A primary difficulty with application of this technique to membranes is that if a significant fraction of the fluorescent molecules are immobile, the focused laser beam may generate a bleached "hole" and subsequent small mechanical motions may then cause fluorescence fluctuations that are not related to molecular number fluctuations. Furthermore, the diffusion must be relatively fast so that a large enough number of data points can be acquired within an experimentally reasonable time scale. Scanning fluorescence correlation spectroscopy circumvents these difficulties; in this type of FCS, the sample is scanned through a focused laser beam or a focused laser beam is scanned through the sample, and the fluorescence fluc-

Received for publication 26 July 1995 and in final form 3 January 1996.
Address reprint requests to Dr. Nancy L. Thompson, Department of Chemistry, University of North Carolina, CB #3290, Chapel Hill, NC 27599-3290. Tel.: 919-962-0328; Fax: 919-962-2388; E-mail: nlt@unc.edu. The present address of Dr. Huang is Los Alamos National Laboratory, Los Alamos, NM.

0006-3495/96/04/2001/07 $2.00

tuations are measured as a function of position (Meyer and Schindler, 1988; St-Pierre and Petersen, 1990, 1992; Petersen et al., 1986). Recently this method has been adapted for use with a laser scanning confocal microscope (Petersen et al., 1993; Koppel et al., 1994) and with two-photon excitation fluorescence microscopy (Berland et al., 1995).

In the imaging FCS (I-FCS) method described herein, a charge-coupled device (CCD) detector was employed to record two-dimensional fluorescence intensity distributions. The pixel-to-pixel fluorescence fluctuations from a single fluorescence image were spatially autocorrelated. A prominent advantage of I-FCS as compared to conventional FCS is that a large number of data points, rather than one, may be collected per sample time. In addition, I-FCS does not require fast diffusion, sample translation, moving optical components, or acquisition of consecutive images. The described method is similar to the one previously used for analyzing acetylcholine receptor clusters on myotubes (Wang and Axelrod, 1994).

MATERIALS AND METHODS

Fluorescent beads

Fluorescein-coated microbeads with two diameters (1 μm and 50 nm) were obtained commercially (Polysciences, Inc., Warrington, PA). Both bead suspensions were dialyzed against phosphate-buffered saline (PBS) (0.05 M sodium phosphate, 0.15 M sodium chloride, 0.01% sodium azide, pH 7.4) and diluted 10-fold with PBS.

Antibodies

Monoclonal anti-trinitrophenyl (TNP) IgE antibodies were purified from supernatants of the hybridoma TIB142 (American Type Culture Collection, Rockville, MD) by affinity chromatography using dinitrophenyl-conjugated human serum albumin (Pisarchick and Thompson, 1990). Antibodies were eluted with 0.01 M *N*-2,4-dinitrophenylglycine (DNP-G) in PBS and were dialyzed extensively against PBS. Polyclonal sheep anti-mouse IgE antibodies were obtained commercially (Calbiochem, La Jolla, CA) and dialyzed into PBS. The IgE antibodies were labeled (R-) with tetramethylrhodamine isothiocyanate (Molecular Probes, Inc., Junction City, OR) as previously described (Timbs and Thompson, 1990). IgE and R-IgE concentrations were determined spectrophotometrically assuming a molecular weight of 184 kDa and the following molar absorptivities: ϵ(IgE, 280 nm) = 298,000 M^{-1} cm^{-1}; ϵ(R, 280 nm)/ϵ(R, 514 nm) = 0.56. The concentrations of tetramethylrhodamine and the molar ratios of tetramethylrhodamine to IgE (0.9–1.5) were calculated using ϵ(R, 556 nm) = 66,000 M^{-1} cm^{-1}.

All antibodies were passed through a 0.2-μm filter and clarified (100,000 × *g*, 0.5 h) no more than 10 h before application to planar membranes. Gel filtration measurements (G200–120 Sephadex; 1.5 cm × 60 cm; flow rate, 0.2 ml/min; sample volume, 1.0 ml; PBS) showed that labeled and unlabeled IgE antibodies (~0.5 mg/ml) eluted with symmetrical peaks and at identical elution volumes, corresponding to IgE monomers. Possible higher-molecular-weight IgE aggregates were not detected.

Phospholipid vesicles

1,2-Dipalmitoyl-*sn*-glycero-3-phosphocholine (DPPC), 1,2-dipalmitoyl-sn-glycero-3-phosphoethanolamine-N-[6[(2, 4, 6-trinitrophenyl)amino]caproyl] (TNP-cap-DPPE), and 1,2-dipalmitoyl-sn-glycero-3-phosphoethanolamine-N-(7-nitro-2-1,3-benzoxadiazol-4-yl) (NBD-DPPE) were obtained commercially (Avanti Polar Lipids, Birmingham, AL) and used without further purification. Small unilamellar vesicles were prepared at 2 mM in PBS from 25 mol% TNP-cap-DPPE and 75 mol% DPPC, as previously described (Pearce et al., 1992). Some vesicles were composed of 100 mol% DPPC, or of 5 mol% NBD-DPPE, 25 mol% TNP-cap-DPPE, and 70 mol% DPPC.

Substrates

Sample chambers were constructed by adhering 24 mm × 60 mm no. 0 microscope coverslips to aluminum holders that contained 0.8″ × 0.8″ apertures, using Sylgard 184 silicone elastomer (Dow Corning Corp., Midland, MI). These holders, as well as fused silica slides (1″ × 1.2″; Quartz Scientific, Fairport Harbor, OH), were cleaned by boiling with Cleaning Solution (ICN, Costa Mesa, CA), bath sonicating, and rinsing extensively with deionized water. Polylysine-coated glass slides (Polysciences) were cleaned by rinsing with ethanol and deionized water. Two strips of single-coated Kapton polyimide adhesive film (0.001″ thickness; Saunders Engineering Corp., Raleigh, NC) were mounted on the coverslips, followed by fused silica slides or polylysine-coated slides. The chambers were held together with aluminum clips.

Sample preparations

Fluorescent beads were deposited on mounted polylysine-coated slides by spontaneous adsorption for 30 min followed by rinsing with 1 ml PBS. Substrate-supported planar membranes were constructed by depositing vesicles on the fused silica surfaces as described previously (Pearce et al., 1992). Vesicles were deposited and fused on substrates by spontaneous adsorption for 25 min followed by rinsing with 2 ml PBS. Planar membranes were then treated with 250 μl PBS containing various concentrations of tetramethylrhodamine-labeled and unlabeled IgE antibodies. For imaging, samples were prepared by diluting labeled IgE five-fold with unlabeled IgE to yield the desired final concentration; for binding curve measurements, samples were prepared with only labeled IgE. After application of antibody solutions, the planar membranes were incubated at room temperature for 30 min and rinsed with 1 ml PBS. Some samples treated with R-IgE were treated further by adding 250 μl of 0.1 mg/ml unlabeled, polyclonal anti-IgE for 30 min and rinsing with 1 ml PBS.

Fluorescence microscopy

The fluorescence microscope was composed of an argon ion laser (Innova 90–6; Coherent, Inc., Palo Alto, CA), an inverted optical microscope (Zeiss Axiovert; Eastern Microscope Co., Raleigh, NC), and a slow-scan cooled CCD (KAF-1400; Photometrics, Tucson, AZ) connected to a personal computer (Gateway 486). The laser beam was directed through a focusing lens (focal length 100 mm) and a cubic fused silica prism [(1.5 cm)^3], and totally internally reflected at the interface of the fused silica or polylysine-coated slides and the solution (Hsieh et al., 1992). Evanescently excited fluorescence was collected through a microscope objective (Nikon, oil-immersion, 60×, NA 1.4) and directed through a dichroic mirror and barrier filter to the CCD.

Images were acquired with the following conditions: wavelength, 488.0 nm for fluorescein-coated beads, 514.5 nm for R-IgE; angle of incidence on the fused silica-solution interface, ~75°; laser power, 5–20 mW; size of illuminated area, ~50 × 200 μm; camera exposure time, 100–500 ms. Because the physical pixel size was (6.8 μm)^2 and the objective was 60×, the pixel size at the sample plane was (0.11 μm)^2. This prediction was confirmed by imaging a calibration slide.

Calculations

Images were corrected for dark counts and truncated to subimages by using the Photometrics CCD software. Corrections for the nonuniform spatial illumination intensities and digital calculations of fluorescence fluctuation

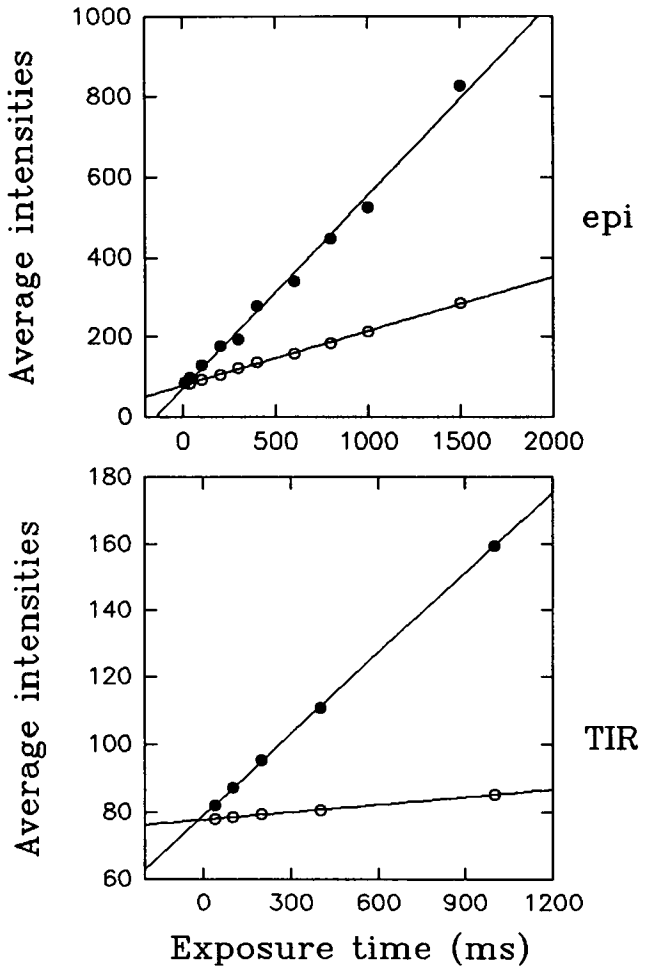

FIGURE 1 Higher signal-to-noise ratio with evanescent illumination. Images obtained with evanescent illumination contain less background as compared to those obtained with epi-illumination. For both epi-illumination and evanescent illumination, the average pixel intensity was plotted as a function of exposure time for both fluorescent and background samples. The fluorescent sample was prepared by treating plasma-cleaned fused silica with 20 μg/ml R-IgE and 80 μg/ml unlabeled IgE in PBS for 30 min, followed by rinsing with 1 ml PBS; the background sample contained only PBS. Images were acquired with the following conditions: laser power, 0.1 W for epi-illumination data, 0.04 W for evanescent illumination data; sample area, 80 × 80 μm^2 for epi-illumination, 80 × 140 μm^2 for evanescent illumination. By defining the signal-to-noise ratio as the ratio of the slopes of the least-square linear regression lines for the fluorescent samples and for the background samples, one finds that this ratio is 10.9 for evanescent illumination and 3.5 for epi-illumination.

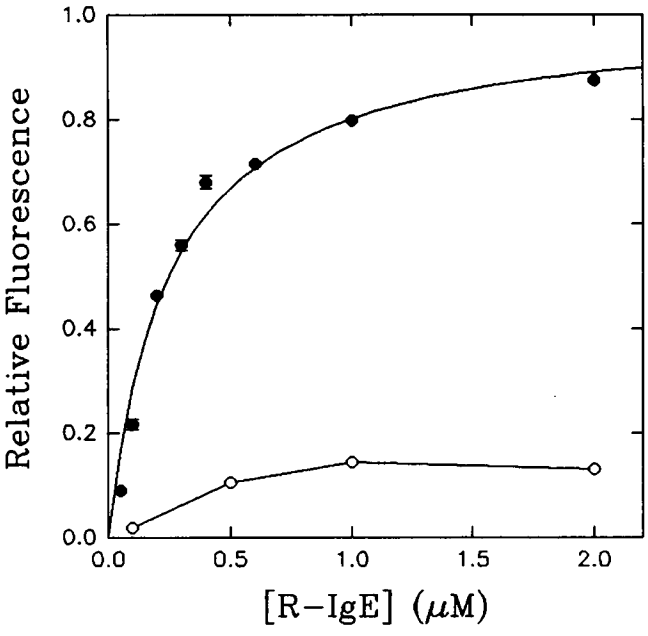

FIGURE 2 Binding curve for R-IgE on planar membranes. This figure shows the evanescently excited fluorescence measured on planar membranes composed of DPPC (75 mol%) and TNP-cap-DPPE (25 mol%) (●). The fluorescence, which is assumed to be proportional to the R-IgE surface density, is plotted as a function of the solution concentration of R-IgE with which membranes were treated before washing. R-IgE binds to the membranes in a saturable manner, with an apparent equilibrium dissociation constant $K_d \approx 0.25$ μM. The evanescently excited fluorescence of DPPC planar membranes treated with R-IgE was much lower (○). Uncertainties are standard deviations for averages over eight spatially independent measurements.

autocorrelation functions were carried out using Fortran routines on a Convex C3840 supercomputer. Calculated autocorrelation functions were fit to theoretical forms with SigmaPlot software.

Data analysis

Raw images were corrected for background by subtracting the averaged dark counts obtained as bias images. Subimages were created from the dark-corrected images by selecting a rectangular area from well within the illuminated region of each image. The subimages typically contained 240 rows and 620 columns, corresponding to a sample area of ~26 μm × 68 μm.

To correct for the Gaussian intensity profile, the dark-corrected images were curve fitted to

$$\ln[f(i,j)] = \sum_{m=1}^{4}\sum_{n=1}^{4} a_{mn} i^{m-1} j^{n-1} \quad (1)$$

$$\ln[f(i,j)] = \sum_{n=1}^{4} b_n(i) j^{n-1} \quad (2)$$

$$b_n(i) = \sum_{m=1}^{4} a_{mn} i^{m-1}, \quad (3)$$

where $f(i,j)$ was the intensity of the pixel at row i and column j. The parameters a_{mn}, with $m \neq 1$ or $n \neq 1$, and $m = 4$ or $n = 4$, were included for modification from an ideal elliptical Gaussian shape (Burghardt and Thompson, 1984). In the curve fitting algorithm, each row of data was first fit to a third-order polynomial versus the column number (j) to give $b_n(i)$ (Eq. 2). Next, the four arrays $b_n(i)$ (for $n = 1$ to 4) were fit to third-order polynomials versus the row number (i) to yield the a_{mn} (Eq. 3). The obtained 16 parameters a_{mn} were used to generate a smoothed image that was the best fit of the dark-corrected subimage to Eq. 1. The images were corrected for the spatially nonuniform excitation intensity by performing a pixel-to-pixel division of the dark-corrected subimages by their smoothed counterparts.

A complexity arose for R-IgE images containing pixels with very high intensities. In these cases, the method described above did not yield an accurately smoothed image. Therefore, a data-screening algorithm in

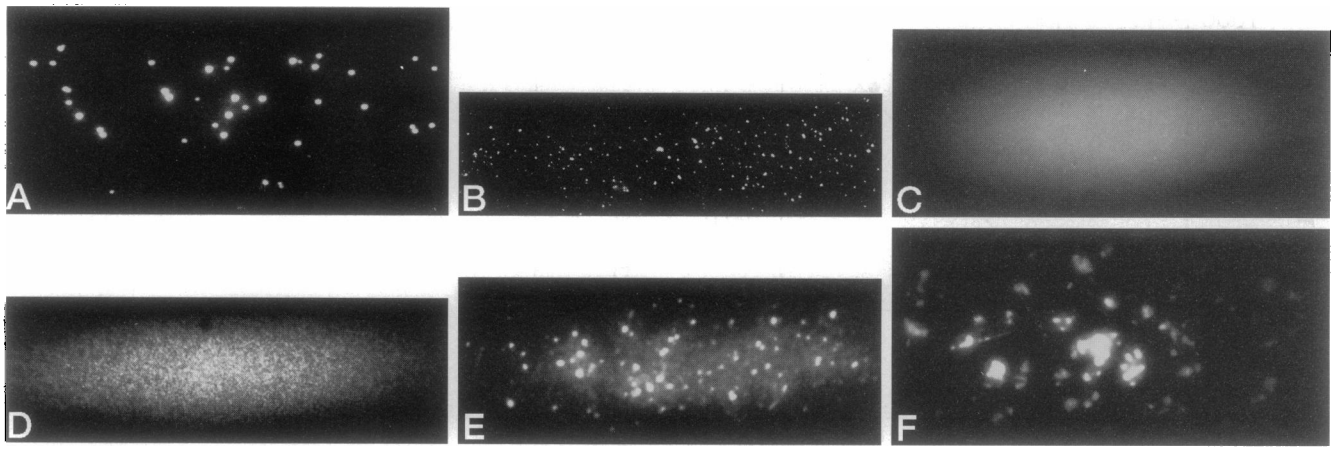

FIGURE 3 Fluorescence images. Images of planar samples of different compositions are visually distinctive. (*a*) Polylysine-coated glass with adsorbed 1-μm fluorescent beads; (*b*) polylysine-coated glass with adsorbed 50-nm fluorescent beads; (*c*) TNP-cap-DPPE/DPPC/NBD-DPPE planar membrane; (*d*) TNP-cap-DPPE/DPPC planar membrane containing a density of R-IgE corresponding to 20% surface saturation; (*e*) TNP-cap-DPPE/DPPC planar membrane containing a density of R-IgE corresponding to 80% surface saturation; (*f*) TNP-cap-DPPE/DPPC planar membranes containing a density of R-IgE corresponding to 60% surface saturation and further treated with anti-IgE.

which a threshold was set to screen out pixels with high intensities was incorporated. For images of fluorescent beads, a similar threshold was set so that only those pixels with intensities above the threshold were retained. The intensities below the threshold were considered background. A final selection was incorporated, for both image types, to ensure that the fitting procedures used only data sets containing more than 10 number pairs after screening.

The spatial fluorescence fluctuation autocorrelation function is defined as

$$G(\rho) = \frac{\langle g(r+\rho)g(r)\rangle - \langle g(r)\rangle^2}{\langle g(r)\rangle^2}, \tag{4}$$

where the brackets indicate a spatial average over the image and $g(r)$ is the fluorescence intensity at position r, corrected for the background and the Gaussian illumination intensity profile. For a corrected subimage with R rows and C columns, $G(\rho)$ was calculated by using

$$\langle g(r)\rangle = [RC]^{-1} \sum_{i=1}^{R} \sum_{j=1}^{C} g(i,j) \tag{5}$$

$$\langle g(r+\rho)g(r)\rangle = [(R-\rho)C + R(C-\rho)]^{-1} \times \sum_{i=1}^{R} \sum_{j=1}^{C} [g(i+\rho,j)g(i,j) + g(i,j+\rho)g(i,j)], \tag{6}$$

where i and j were the row and column numbers and $g(i,j)$ was the corrected intensity at pixel (i,j). Those $g(i,j)$ for which $i > R$ and $j > C$ were assumed to be zero. $G(\rho)$ were calculated for $\rho = 0$ to 50. The procedure averages over possible azimuthal asymmetries that may be present in the images.

RESULTS AND DISCUSSION

Sample illumination was provided by the evanescent field of a totally internally reflected laser beam. Evanescent illumination generated less background light as compared to epi-illumination (Fig. 1). Evanescent illumination also minimized the spatial intensity fluctuations often observed with epi-illumination that result from passage of the excitation light through the internal components of an optical microscope.

The evanescently excited fluorescence of R-IgE on planar membranes (25 mol% TNP-cap-DPPE, 75 mol% DPPC) was measured as a function of the solution concentration of R-IgE with which planar membranes were incubated. As shown in Fig. 2, the fluorescence increased with the R-IgE solution concentration and reached saturable levels at high

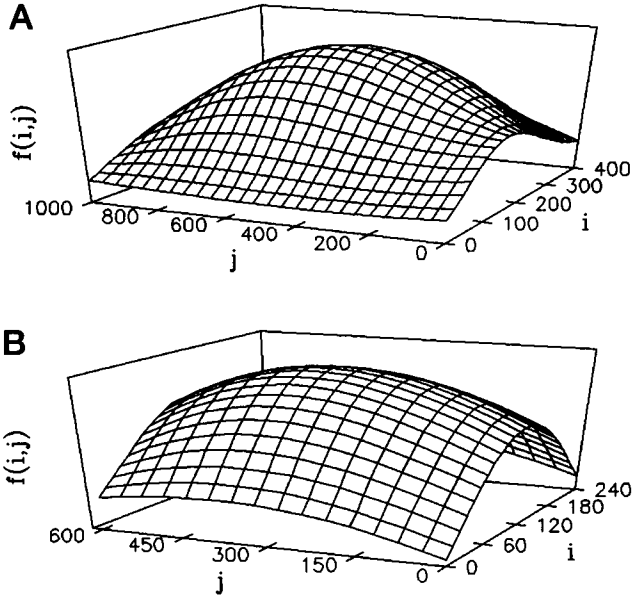

FIGURE 4 Smoothed images. Smoothed images were generated by curve fitting to Eqs. 1–3 as described in the text. Shown here are the smoothed versions of two of the images shown in Fig. 3. (*a*) The smoothed version of Fig. 3 *a*; (*b*) the smoothed version of Fig. 3 *d*.

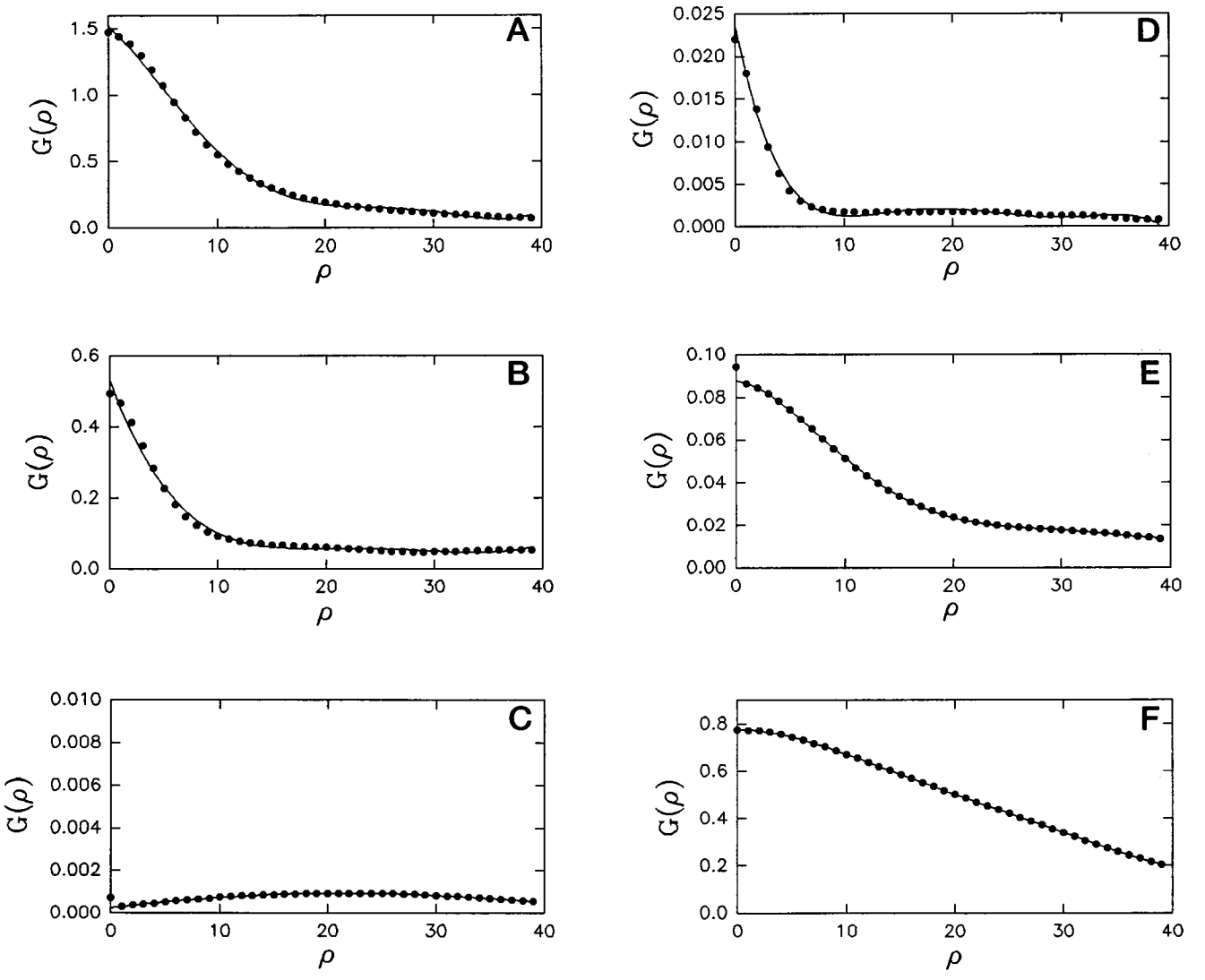

FIGURE 5 Fluorescence fluctuation autocorrelation functions. Functions G(ρ) were calculated from images that had been corrected for background and for the spatially nonuniform illumination as described in text. Shown here are the autocorrelation functions of the images shown in Fig. 3, along with the best fits to fifth-order polynomials in ρ: (*a*) polylysine-coated glass with adsorbed 1-μm fluorescent beads; (*b*) polylysine-coated glass with adsorbed 50-nm fluorescent beads; (*c*) TNP-cap-DPPE/DPPC/NBD-DPPE planar membrane; (*d*) TNP-cap-DPPE/DPPC planar membrane containing a density of R-IgE corresponding to 20% surface saturation; (*e*) TNP-cap-DPPE/DPPC planar membrane containing a density of R-IgE corresponding to 80% surface saturation; (*f*) TNP-cap-DPPE/DPPC planar membranes containing a density of R-IgE corresponding to 60% surface saturation and further treated with anti-IgE.

solution concentrations. In contrast, the fluorescence of R-IgE on 100 mol% DPPC membranes was much lower in magnitude. Thus, the binding of R-IgE to planar membranes required its specific hapten (TNP). The best fit of the data in Fig. 2 to the shape for a simple surface binding curve (e.g., Hsieh et al., 1992) gave an apparent equilibrium dissociation constant of $K_d \approx 0.25$ μM. Thus, the R-IgE solution concentrations corresponding to 20%, 40%, 60%, and 80% surface saturation were 0.062 μM, 0.17 μM, 0.38 μM, and 1.0 μM, respectively. Fluorescence images were obtained for these four conditions.

Fig. 3, *a* and *b*, shows typical fluorescence images of fluorescent beads with 1 μm and 50 nm diameters, respectively. Images of membranes containing 5 mol% NBD-DPPE appeared uniform (Fig. 3 *c*). The broad elliptical shape was due to the spatial dependence of the illumination intensity. Fig. 3 *d* shows a typical fluorescence image of a TNP-cap-DPPE/DPPC planar membrane containing bound R-IgE at 20% of the saturating density. As shown, the spatial distribution of R-IgE was not uniform. The nonuniformities appeared to be several pixels wide and therefore of a size approximately equal to optical resolution. The images of membranes with 40% and 60% R-IgE surface saturations appeared similar to those with 20% saturation and are not shown. The images for 80% saturation (Fig. 3 *e*) showed larger nonuniformities and higher contrasts in intensity between dark and bright regions. Some of the R-IgE samples with 60% surface saturation were treated with 0.1 mg/ml

TABLE 1 Parameters G(0) and σ

Surface	Fluorescent component	G(0)	$\sigma(\mu m)$	n
Polylysine-coated glass	1-μm beads	1.62 ± 0.20	0.844 ± 0.022	10
Polylysine-coated glass	50-nm beads	0.39 ± 0.20	0.484 ± 0.043	10
Planar membrane	NBD-DPPE	0.00128 ± 0.00018	—	15
Planar membrane	R-IgE 20% saturation	0.0146 ± 0.0021	0.496 ± 0.063	13
Planar membrane	R-IgE 40% saturation	0.00782 ± 0.00056	0.595 ± 0.095	12
Planar membrane	R-IgE 60% saturation	0.0096 ± 0.0014	0.66 ± 0.12	19
Planar membrane	R-IgE 80% saturation	0.074 ± 0.015	1.05 ± 0.09	18
Planar membrane	R-IgE 60% saturation with anit-IgE	0.50 ± 0.19	3.33 ± 0.64	4

The extrapolated values of G(0) and the correlation distances σ were obtained by curve fitting the autocorrelation functions $G(\rho)$ to fifth-order polynomials. Parameters values are given as the average of those calculated from a number of images n. Uncertainties are standard deviations for averages over the n independently acquired images.

unlabeled anti-IgE. Images of these samples (Fig. 3 *f*) suggested that, as expected, the anti-IgE induced larger and brighter clusters.

Fluorescence fluctuation autocorrelation functions were calculated from images as described above. Fig. 4, *a* and *b*, shows two representative smoothed images. The smoothed images were approximately elliptically Gaussian in shape. Fig. 5*a–f* shows typical functions $G(\rho)$. The values of $G(\rho)$ shown in these plots were calculated from the images shown in Fig. 3*a–f*.

Because the rate and shape of decay for the $G(\rho)$ were dependent on the (unknown) size and shape of the aggregation entities, the functions were curve fitted to fifth-order polynomials (excluding the G(0) values that contained shot noise). This analysis generated two useful parameters. The extrapolated initial value, G(0), was related to the average cluster intensity and density. The correlation distance, σ, defined as the distance at which $G(\rho)$ dropped to one-half of the initial value, was related to the average cluster size. Table 1 summarizes the obtained values of G(0) and σ.

The values of G(0) calculated from images of fluorescent beads were large, and the values of G(0) were negligible for planar membranes containing fluorescent lipids, as expected. G(0) was measurable and approximately equivalent for membranes 20%-60% saturated with R-IgE, increased significantly for membranes 80% saturated with R-IgE, and increased again in the presence of unlabeled anti-IgE.

The correlation distance σ for 1-μm beads agreed well with the known value (Table 1). However, the correlation distance for 50-nm beads was significantly higher than the known bead diameter. This latter result may be attributed to the optical transfer function of the microscope. Therefore, for fluorescent entities smaller than optical resolution, I-FCS does not directly yield accurate information about cluster size via the parameter σ. However, this result does mean that (advantageously) I-FCS will be applicable to small molecular clusters (such as receptor dimers) because spatial correlations will exist for several pixels and these correlations can be used to calculate extrapolated values of G(0). The correlation distances for planar membranes 20%, 40%, and 60% saturated with R-IgE were only slightly larger than the measured correlation distance for 50-nm beads, indicating that the average IgE cluster size in these samples was smaller than or approximately equal to optical resolution. Significantly higher values of σ were found for membranes 80% saturated with R-IgE or treated with both R-IgE and anti-IgE.

SUMMARY

This paper demonstrates the feasibility of using a CCD detector with spatial fluorescence fluctuation autocorrelation (I-FCS) for detecting and characterizing molecular clusters in model and natural cell membranes. An advantage of I-FCS as compared to conventional FCS is that a large number of data points, rather than one, may be collected per sample time. In addition, I-FCS does not require fast diffusion, sample translation, moving optical components, or acquisition of consecutive images. We have shown that, as a result of the microscope's optical transfer function, appreciable spatial correlations persist for several pixels, even when fluorescent entities are smaller than optical resolution. This result means that the values of G(0) may be determined by extrapolation from values of $\rho > 0$, eliminating the complications due to shot noise that would be encountered by direct analysis of the G(0) values. In a future work, the use of high-order fluorescence fluctuation autocorrelation with I-FCS will be examined (Vanden Broek et al., manuscript in preparation).

We thank Arthur G. Palmer of Columbia University for helpful conversations.

This work was supported by National Institutes of Health grant GM-37145 and by National Science Foundation grant DMB-9024028.

REFERENCES

Berland, K. M., P. T. C. So, and E. Gratton. 1995. Two-photon fluorescence correlation spectroscopy: method and application to the intracellular environment. *Biophys. J.* 68:694–701.

Bormann, B. J., and D. M. Engelman. 1992. Intramembrane helix-helix association in oligomerization and transmembrane signaling. *Annu. Rev. Biophys. Biomol. Struct.* 21:223–242.

Burghardt, T. P., and N. L. Thompson. 1984. Evanescent intensity of a focused Gaussian light beam undergoing total internal reflection in a prism. *Opt. Eng.* 23:62–67.

Cunningham, B. C., M. Ultsch, A. M. de Vos, M. G. Mulkerrin, K. R. Caluser, and J. A. Wells. 1991. Dimerization of the extracellular domain of the human growth hormone receptor by a single hormone molecule. *Science.* 254:821–825.

Fantl, W. J., D. E. Johnson, and L. T. Williams. 1993. Signalling by receptor tyrosine kinases. *Annu. Rev. Biochem.* 62:453–481.

Ghosh, R. N., and W. W. Webb. 1994. Automated detection and tracking of individual and clustered cell surface low density lipoprotein receptor molecules. *Biophys. J.* 66:1301–1318.

Grasberger, B., A. P. Minton, C. DeLisi, and H. Metzger. 1986. Interaction between proteins localized in membranes. *Proc. Natl. Acad. Sci. USA.* 83:6258–6262.

Hsieh, H. V., C. L. Poglitsch, and N. L. Thompson. 1992. Direct measurement of the weak interactions between a mouse Fc receptor (FcγRII) and IgG1 in the absence and presence of hapten: a total internal reflection fluorescence microscopy study. *Biochemistry.* 31:11562–11566.

Jans, D. A. 1992. The mobile receptor hypothesis revisited: a mechanistic role for hormone receptor lateral mobility in signal transduction. *Biochim. Biophys. Acta.* 1113:271–276.

Jap, B. K., M. Zulauf, T. Scheybani, A. Hefti, W. Baumeister, U. Aebi, and A. Engel. 1992. 2D crystallization: from art to science. *Ultramicroscopy.* 46:45–84.

Koppel, D. E., F. Morgan, A. E. Cowan, and J. H. Carson. 1994. Scanning concentration correlation spectroscopy using the confocal laser microscope. *Biophys. J.* 66:502–507.

Kornberg, R., and S. Darst. 1991. Two-dimensional crystals of proteins on lipid layers. *Curr. Opin. Struct. Biol.* 1:642–646.

Kubitscheck, U., M. Kircheis, S. R. Schweitzer, W. Dreybrodt, T. M. Jovin, and I. Pecht. 1991. Fluorescence resonance energy transfer on single living cells. *Biophys. J.* 60:307–318.

Kubitscheck, U., S. R. Schweitzer, D. J. Arndt-Jovin, T. M. Jovin, and I. Pecht. 1993. Distribution of type I Fc epsilon-receptors on the surface of mast cells probed by fluorescence resonance energy transfer. *Biophys. J.* 64:110–120.

Liang, X. H., M. Volkmann, R. Klein, B. Herman, and S. J. Lockett. 1993. Co-localization of the tumor-suppressor protein p53 and human papillomavirus E6 protein in human cervical carcinoma cell lines. *Oncogene.* 8:2645–2652.

Matayoshi, E. D., W. H. Sawyer, and T. M. Jovin. 1991. Rotational diffusion of band 3 in erythrocyte membranes. 2. Binding of cytoplasmic enzymes. *Biochemistry.* 30:3538–3543.

Meyer, T., and H. Schindler. 1988. Particle counting by fluorescence correlation spectroscopy: simultaneous measurement of aggregation and diffusion of molecules in solution and in membranes. *Biophys. J.* 54: 983–993.

Morrison, I. E. G., C. M. Anderson, G. N. Georgiou, G. V. W. Stevenson, and R. J. Cherry. 1994. Analysis of receptor clustering on cell surface by imaging fluorescent particles. *Biophys. J.* 67:1280–1290.

Palmer, A. G., III, and N. L. Thompson. 1989a. High-order fluorescence fluctuation analysis of model protein clusters. *Proc. Natl. Acad. Sci. USA.* 86:6148–6152.

Palmer, A. G., III, and N. L. Thompson. 1989b. Fluorescence correlation spectroscopy for detecting submicroscopic clusters of fluorescent molecules in membranes. *Chem. Phys. Lipids.* 50:253–270.

Pearce, K. H., R. G. Hiskey, and N. L. Thompson. 1992. Surface binding kinetics of prothrombin fragment 1 on planar membranes measured by total internal reflection fluorescence microscopy. *Biochemistry.* 31: 5983–5995.

Petersen, N. O., P. L. Hoddelius, P. W. Wiseman, O. Seger, and K. E. Magnusson. 1993. Quantitation of membrane receptor distributions by image correlation spectroscopy: concept and application. *Biophys. J.* 65:1135–1146.

Petersen, N. O., D. C. Johnson, and M. J. Schlesinger. 1986. Scanning fluorescence correlation spectroscopy. II. Application to virus glycoprotein aggregation. *Biophys. J.* 49:817–820.

Pisarchick, M. L., and N. L. Thompson. 1990. Binding of a monoclonal antibody and its Fab fragment to supported phospholipid monolayers measured by total internal reflection fluorescence microscopy. *Biophys. J.* 58:1235–1249.

Sette, A., J. Alexander, J. Ruppert, K. Snoke, A. Franco, G. Ishioka, and H. M. Grey. 1994. Antigen analogs/MHC complexes as specific T cell receptor antagonists. *Annu. Rev. Immunol.* 12:413–431.

St-Pierre, P. R., and N. O. Petersen. 1990. Relative ligand binding to small or large aggregates measured by scanning correlation spectroscopy. *Biophys. J.* 58:503–511.

St-Pierre, P. R., and N. O. Petersen. 1992. Average density and size of microclusters of epidermal growth factor receptors on A431 cells. *Biochemistry.* 31:2459–2463.

Szabo, G., Jr., P. S. Pine, J. L. Weaver, M. Kasari, and A. Aszalos. 1992. Epitope mapping by photobleaching fluorescence resonance energy transfer measurements using a laser scanning microscope system. *Biophys. J.* 61:661–670.

Thompson, N. L. 1991. Fluorescence correlation spectroscopy. *In* Topics in Fluorescence Spectroscopy, Vol. 1. J. R. Lakowicz, editor. Plenum Press, New York.

Timbs, M. M., and N. L. Thompson. 1990. Slow rotational mobilities of antibodies and lipids associated with substrate-supported phospholipid monolayers as measured by polarized fluorescence photobleaching recovery. *Biophys. J.* 58:413–428.

Ullrich, A., and J. Schlessinger. 1990. Signal transduction by receptors with tyrosine kinase activity. *Cell.* 61:203–212.

Velez, M., K. F. Barald, and D. Axelrod. 1990. Rotational diffusion of acetylcholine receptors on cultured rat myotubes. *J. Cell Biol.* 110: 2049–2059.

Wang, M. D., and D. Axelrod. 1994. Microclustering patterns of acetylcholine receptors on myotubes studies by spatial fluorescence autocorrelation. *Bioimaging.* 2:22–35.

Ward, M. D., and D. A. Hammer. 1992. Morphology of cell-substratum adhesion. Influence of receptor heterogeneity and nonspecific forces. *Cell Biophys.* 20:177–222.

Wright, L. L., A. G. Palmer, and N. L. Thompson. 1988. Inhomogeneous translational diffusion of monoclonal antibodies on phospholipid Langmuir-Blodgett films. *Biophys. J.* 54:463–470.

Young, R. M., J. K. Arnette, D. A. Roess, and B. G. Barisas. 1994. Quantitation of fluorescence energy transfer between cell surface proteins via fluorescence donor photobleaching kinetics. *Biophys. J.* 67: 881–888.

Young, J. D., J. C. Unkeless, T. M. Young, A. Mauro, and Z. A. Cohn. 1983. Role for mouse macrophage IgG Fc receptor as ligand-dependent ion channel. *Nature.* 306:186–189.

Zidovetzki, R., D. A. Johnson, D. J. Arndt-Jovin, and T. M. Jovin. 1991. Rotational mobility of high-affinity epidermal growth factor receptors on the surface of living A431 cells. *Biochemistry.* 30:6162–6166.